Resistivity anisotropy from the multiorbital Boltzmann equation in nematic FeSe

Marco Marciani and Lara Benfatto

Department of Physics and ISC-CNR, "Sapienza" University of Rome, P.le A. Moro 5, 00185 Rome, Italy

We compute the resistivity anisotropy in the nematic phase of FeSe from the static solution of the multiorbital Boltzmann equation. By introducing disorder at the level of the microscopic multiorbital model we show that even elastic scattering by localized impurities may lead to nontrivial anisotropic renormalization of the electronic velocities, challenging the usual understanding of transport based only on cold- and hot-spots effects. Our model takes into account both the xz/yz and the recently proposed xy nematic ordering. We show that the latter one has a crucial role in order to reproduce the experimentally measured anisotropy, providing a direct fingerprint of the different nematic scenarios on the bulk transport property of FeSe.

I. INTRODUCTION

Among iron-based superconductors, FeSe has a rather unique behavior, due to the presence of a marked nematic transition that occurs without concomitant long-range antiferromagnetic order [1,2]. In FeSe nematicity develops below the temperature $T_s = 90$ K where the lattice undergoes a transition from tetragonal to orthorhombic structure. This metallic state is named nematic because the observed electronic anisotropy, as measured, e.g., by dc transport, is much larger than what expected from the lattice anisotropy [1,2]. In most iron pnictides the structural transition precedes or coincides with the magnetic transition at T_N, below which long-range antiferromagnetic order sets in [3]. The magnetic transition itself is generically ascribed to a nesting mechanism, favored by the similar size among the holelike electronic pockets at Γ and the electronlike electronic pockets around $\mathbf{Q}_X = (\pi, 0)$ and $\mathbf{Q}_Y = (0, \pi)$ in the 1-Fe Brillouin zone (BZ) notation, see Fig. 1. As a consequence, one of the earliest proposals [4,5] identified the nematic phase as a precursor of the magnetic one, such that spins are still disordered but spin fluctuations at momentum $\mathbf{Q}$ break the C_4 lattice rotational symmetry, becoming stronger at $\mathbf{Q}_X$ than at $\mathbf{Q}_Y$. Even though this view does not necessarily imply the existence of long-range magnetic order at a $T_N < T_s$, the lack of magnetic transition in FeSe, along with the experimental observation of a marked Fermi-surface reconstruction below T_s, triggered also alternative proposals, based on an orbital-ordering scenario [6–10]. The two paradigms are actually not necessarily alternative, since also a spin-nematic scenario can lead to an effective orbital ordering once one correctly includes the orbital content of the spin fluctuations themselves, within the so-called orbital-selective spin-fluctuation scenario (OSSF) [11–13].

From the experimental point of view the systematic investigation of the band structure of FeSe by means of ARPES revealed a sizable deformation of the Fermi surface, which can be described via a momentum-dependent crystal-field splitting of the d_{xz}, d_{yz}, d_{xy} orbitals contributing to the low-energy Fermi pockets [12,14–21]. Above T_s the Fermi surface of FeSe

at $k_z = 0$ consists of one circular holelike pocket at Γ with xz and yz character, and two electronlike pockets at X and Y with xy and, respectively, yz and xz character [see Fig. 1(b)], while an additional holelike pocket at Z appears at $k_z = \pi/c$. So far, there is general consensus about the existence of a xz/yz splitting that changes sign in going from the Brillouin-zone center to momenta around $\mathbf{Q}_X$ or $\mathbf{Q}_Y$. This can be represented by a nematic order parameter

$$\Phi^{xz/yz} = \langle d_{xz}^\dagger d_{xz} - d_{yz}^\dagger d_{yz} \rangle, \tag{1}$$

that is positive at Γ and negative at X and Y.

On the other hand, the exact role of the xy orbital is still debated. Such a debate comes along with the ongoing discussion on the presence or not of the Y electron pocket below T_s [12,17–22], which is also relevant for the theoretical interpretation of the gap anisotropy observed in the superconducting state [13,23–27]. The main point is that accounting only for the xz/yz splitting in Eq. (1) a large electron pocket with mixed yz and xy character is expected at the Y point [see Fig. 1(c)]. However, such a pocket has not been resolved in the most recent ARPES measurements in detwinned samples [17,19,20]. In order to solve this puzzle [21] an alternative scenario has been recently suggested in Ref. [28], where the authors proposed an additional nematic order parameter accounting for the splitting of the xy occupancy in the two electron pockets, i.e.,

$$\Phi^{xy} = \langle d_{xy,X}^\dagger d_{xy,X} - d_{xy,Y}^\dagger d_{xy,Y} \rangle. \tag{2}$$

Such an order parameter is equivalent to an anisotropic hopping between the d_{xy} orbitals of the nearest-neighbors atoms in the 2-Fe unit cell, which is the physical one. The main consequence of the splitting (2) is to readily explain the progressive disappearance of the Y pocket at a temperature below T_s [see Fig. 1(d)], accompanied by a Lifshitz transition.

A second striking difference among FeSe and other families of iron-based superconductors is the different sign of the resistivity anisotropy reported below T_s. Indeed, while in
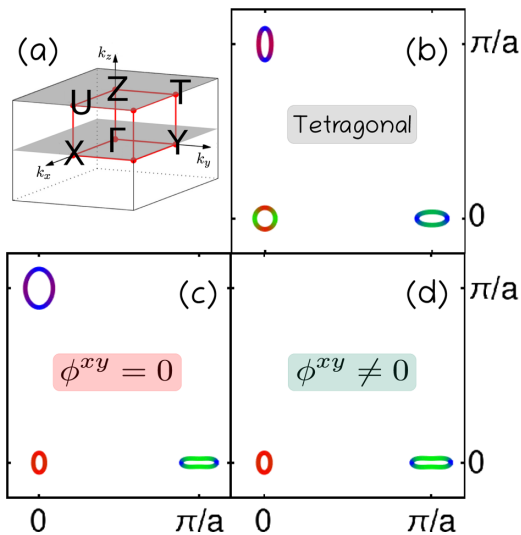
FIG. 1. 1-Fe Brillouin Zone(BZ) in different regimes. (a) Nomenclature of the pocket centers in the unfolded three-dimensional (3D) BZ corresponding to 1Fe atom per unit cell; the gray planes mark the sheets at $k_z = 0$ and $k_z = \pi/c$. (b)–(d) Fermi surface topology of FeSe in the 1-Fe BZ at $k_z = 0$, in the normal state (b) and in the nematic phase (c), (d). (c) corresponds to the Fermi surface expected in the presence only of the (xz, yz) nematic order parameter (1), while (d) corresponds to the Fermi surface obtained by including also the xy order parameter (2). We assume a unique lattice spacing a in the xy plane.

122 compounds [29–34] the resistivity is smaller along the longer a axis (corresponding to the Γ-X direction in the 1-Fe BZ), i.e., $\Delta\rho = \rho_x - \rho_y < 0$, in FeSe the opposite behavior is observed [35,36]. Accounting for such a difference is far from being straightforward, since the dc conductivity of a multiband metal as iron pnictides is controlled by a delicate balance among Fermi velocities, density of states and scattering rates in the various pockets. In such a situation different theoretical proposals pointed out alternatively a prominent role either of the scattering-rate anisotropy [37–42] or of the Fermi-surface deformation [43–45]. The former approach relies mainly on the calculation of the inelastic scattering rate due to the exchange of spin fluctuations, whose anisotropy is ascribed either to the spin-nematic nature of the spin fluctuations [37,41,46] or to a secondary effect of orbital ordering [42]. The predominant role of the Fermi-surface deformation was instead motivated mainly by the analysis of the nematic anisotropy at finite frequency [44,45,47], which involves in principle both the scattering-rate and the plasma-frequency anisotropy. Such an analysis is, however, rather delicate, since from one side the two quantities are unavoidably entangled by causality relations [41], and from the other side one should definitively take into account how interactions having a predominant interband character, as it would be the case for spin fluctuations in iron pnictides, modify the sum-rule behavior as compared to the standard case where interactions have predominant intraband character [48,49].

In general, in a system such as FeSe where orbital reconstruction is much more severe than in 122 compounds, a reasonable starting point to model transport should

definitively account for the Fermi-surface nematicity. A recent calculation within the OSSF scenario pointed out that in general the Fermi-surface reconstruction and the scattering-rate anisotropy give opposite contributions to the resistivity anisotropy [50]. In such a situation, the overall sign of the dc anisotropy is a matter of quantitative balance that requires a thoughtful calculation where all effects are properly accounted for on the same footing.

The present paper aims at achieving this goal within a simplified but yet relevant case, i.e., solving the Boltzmann transport equation in the presence only of elastic scattering processes due to impurities, but within a full orbital model, which describes the Fermi-surface reconstruction as measured experimentally by ARPES. As compared with previous theoretical work [37,46], which analyzed the problem within the band language, we will show that, by correctly accounting for the orbital character of the Fermi pockets, the dc conductivity computed at the level of Boltzmnann equation has a nontrivial behavior. Indeed, as recently discussed for a generic multiorbital case in Ref. [51], while in a single-band system the transport scattering time for isotropic impurities coincides with the quasiparticle one, in a multiorbital system this is not the case. Here the multiorbital composition of the electronic bands plays a role analogous to the momentum dependence of the scattering potential for the single-band system, with two main implications. First, even elastic scattering by isotropic impurities may induce anisotropy in the observables, an effect that has not been included in previous works focused mainly on inelastic processes [37,46]. Second, the renormalization of the current with respect to the bare band velocity, which is equivalent to include the so-called vertex corrections within the standard Kubo approach [52], is finite. In this paper by taking advantage of the semianalytical solution of the multiorbital problem recently provided in Ref. [51] we will compute the dc anisotropy in FeSe testing the two nematic scenarios discussed above, where either the xy nematic order parameter (2) is included or not. We will show that in both cases the velocities renormalization due to disorder significantly contributes to the resistivity anisotropy, and becomes crucial to account for the experimental observations. More specifically, we will show that the recent proposal [28] of a d_{xy} nematicity emerging along with the well-established xz/yz one seems to provide a key ingredient to explain the observed resistivity anisotropy in FeSe. Our results show a direct fingerprint on a bulk material property of the xy nematicity, that should be considered along with its impact on the surface ARPES probe, recently reviewed by Rhodes *et al.* [21].

The plan of the paper is as follows. In Sec. II we introduce the low-energy orbital Hamiltonian. In Sec. III we discuss the Boltzmann equation for the multiorbital model in the presence of disorder and we summarize the main results of the recent theoretical derivation [51] of a semianalytical solution of the integral equation for the renormalized velocities. In Sec. IV we show numerical results for FeSe in the case where both $\Phi^{xz/yz}$ and Φ^{xy} nematic order parameters are present, and we further discuss our results in Sec. V along with the concluding remarks. The Appendixes contain details of the theory and explore different parameter and disorder regimes.

II. THREE-ORBITAL MODEL

To describe FeSe we use a three-orbital low-energy effective model [53], as properly tailored in Ref. [28] to fit ARPES data [22]. Only three spinfull d orbitals are retained, whose creation operators we collect in the vector $\Psi_s = (d_s^{xz}, d_s^{yz}, d_s^{xy})^T$. Thus the Hamiltonian, expanded at momenta close to the pockets centers, reads as:

$$H_T = \sum_{\mathbf{k}\sigma} \Psi_{\mathbf{k}\sigma}^\dagger (H_{\mathbf{k},\sigma}^0 + H_T^\Phi - \mu_T) \Psi_{\mathbf{k}\sigma}, \qquad (3)$$

where μ is the chemical potential; H^0 contains the temperature-independent uncorrelated Hamiltonian; H^Φ accounts for the nematic deformation of the band structure and it is assumed to be independent of the local quasimomentum and spin, but dependent on the temperature T through the order parameters $\Phi_T = \Phi_0 \sqrt{1 - T/T_s}$. Within the OSFF scenario [11–13] such a temperature scaling arises naturally, since H^Φ encodes the real part of the nematic self-energy corrections due to exchange of spin fluctuations among holelike and electronlike pockets. However, at the level of the present computation these can be seen as phenomenological parameters used to reproduce the ARPES data, in the same spirit of Ref. [28].

In FeSe the Fermi pockets are almost cylindrical in the direction perpendicular to the FeSe planes. This allows us to approximate the Fermi pockets as a stack of two cylinders with different basis whose geometrical centers are located, respectively, at the points Γ and X, Y and at the points Z and U, T of the 1-Fe Brillouin zone (BZ), see Fig. 1(a). Being the dispersion weakly k_z dependent, we further simplify the three-dimensional (3D) BZ as the sum of two 2D BZs at $k_z = 0, \frac{\pi}{c}$ and take only the cylinders bases as the relevant 2D pockets (c is the lattice spacing along z axis and we can assume a unique lattice spacing a along the xy plane also in the nematic phase). Thus, the sum $\sum_{\mathbf{k};\sigma}$ over BZ states in Eq. (3) due to these simplifications is equivalent to $L_z/(2c) \sum_{k_x,k_y;k_z=0,\frac{\pi}{c};\sigma}$, with L_z the thickness of the sample. Another simplification occurs. At each pocket only two out of three spinfull orbitals contributes to the physics at the Fermi energy. Thus, at momenta close to the points Γ, X, Y we are allowed to remove from the spinor Ψ the orbitals d^{xy}, d^{xz}, d^{yz}, respectively, and the effective Hamiltonian is described as a 4×4 matrix. The self-energy corrections at different points of the BZ at $k_z = 0$ are explicitly given by (at $k_z = \frac{\pi}{c}$ expressions are formally the same but the parameter values are different):

$$H_T^{\Phi\,\Gamma} = \Phi_T^h\,\tau_3 \otimes \sigma_0,$$

$$H_T^{\Phi\,X/Y} = \left(\frac{\Delta\epsilon_T^{xy}}{2} \pm \frac{\Phi_T^e - \Phi_T^{xy}}{2}\right)\tau_0 \otimes s_0$$

$$\qquad - \left(\frac{\Delta\epsilon_T^{xy}}{2} \mp \frac{\Phi_T^e + \Phi_T^{xy}}{2}\right)\tau_3 \otimes s_0, \qquad (4)$$

where the Pauli matrices τ acts on the relevant orbital space and s on the spin one. The $\Phi^{h(e)}$ parameter here corresponds to the values of $\Phi^{xz/yz}$ near Γ (X or Y), see Eq. (1). The most relevant new parameters introduced in Ref. [28] are the nematic order parameter (2), Φ^{xy}, and a phenomenological energy shift $\Delta\epsilon^{xy}$ of the d^{xy} orbital, which also sets in at the nematic transition. The latter parameter can be regarded, from

a microscopical point of view, as a Hartree shift of the d_{xy} orbital possibly arising from the same interactions responsible for the Φ^{xy} nematic order parameter. Both Φ^{xy} and $\Delta\epsilon^{xy}$ are responsible in general for the lowering (raising) of the band near the X (Y) pocket, since their effects sum up at the Y pocket and partly compensate at the X pocket. The full effective Hamiltonian, the symmetries analysis [53] and all parameter values are presented in Appendix A.

Lowering the temperature from T_s, three Lifshitz transitions take place. Right below T_s there are one pocket at Γ, two pockets at Z (we distinguish the inner from the outer one naming them Z_{in} and Z_{out}), two pockets at X and Y, and two pockets at U and T. Lowering further the temperature the pockets at Y and T disappear simultaneously, at $T \simeq 70$, followed by Z_{in}, at $T \simeq 45$, and only four pockets are present when superconductivity sets in at $T_c = 7$ K. In Fig. 2 below we report the pocket details right at T_s and at T_c, which represents the lower temperature bound for our calculations, which do not include superconducting effects. In the absence of the xy nematic order parameter (2) the pockets at T_c are shown in Fig. 7, for the set of parameters detailed in the Appendix D. In this case the Y pocket survives below T_s and increases in size, as a consequence of the xz/yz nematicity. As we will see below, the resulting resistivity anisotropy has a completely different behavior as compared to the case when also the xy nematic order parameter is present.

III. BOLTZMANN EQUATION

We employ the static homogeneous multiorbital Boltzmann equation to describe the dc electric transport. In its general form the equation reads as [52,54–58]:

$$e\,\mathbf{E} \cdot \nabla_{\mathbf{k}}\,\rho_{\mathbf{k},b} = \sum_{\mathbf{k}',b'} Q_{\mathbf{k},\mathbf{b}}^{\mathbf{k}',\mathbf{b}'}(\rho_{\mathbf{k},b} - \rho_{\mathbf{k}',b'}), \quad 1 \leqslant b \leqslant N_b, \quad (5)$$

where $\rho_{\mathbf{k},b}$ is the electronic density at quasimomentum $\mathbf{k}$ and band b; the number of bands N_b includes the spin degree of freedom. We set $\hbar = 1$ in formulas. We will assume that the collision kernel $Q_{\mathbf{k}\mathbf{k}'}^{bb'}$ includes only elastic scattering coming from unit-cell-localized impurities, located randomly in the sample. Such impurities affect only the local chemical potential (see Appendix B for details). To test the robustness of our results, other disorder types are considered in the Appendix C. The rates $\Gamma_{\mathbf{k},b}$ and the lifetimes $\tau_{\mathbf{k},b}$ of each state are defined as

$$\Gamma_{\mathbf{k},b} = 1/\tau_{\mathbf{k},b} = \sum_{\mathbf{k}',b'} Q_{\mathbf{k}\mathbf{k}'}^{bb'}. \qquad (6)$$

To compute the dc conductivity one needs to find the change $\rho_{\mathbf{k},b}^{\mathbf{E}}$ in the distribution at linear order in the field, that can be expressed in full generality in terms of the renormalized velocities $\mathbf{w}_{\mathbf{k},b}$ as $\rho_{\mathbf{k},b}^{\mathbf{E}} = e\mathbf{E} \cdot \mathbf{w}_{\mathbf{k},b}\,\tau_{\mathbf{k},b}\,\partial_{\varepsilon_{\mathbf{k}}^b} f_{\varepsilon_{\mathbf{k},b}}$, with f_ε the Fermi function. The renormalized velocities differ in general from the bare band velocity defined as $\mathbf{v}_{\mathbf{k}}^b = \nabla_{\mathbf{k}}\varepsilon_{\mathbf{k}}^b$. The former can be computed easily if the so-called relaxation-time approximation [46,51,52,59,60] is implemented. This is justified whenever $\mathbf{w}$ and $\mathbf{v}$ are (at least approximately) parallel, e.g., due to some symmetry of the system, with a coefficient of proportionality set by the so-called transport scattering rate. In most cases such as the one at hand, however, the
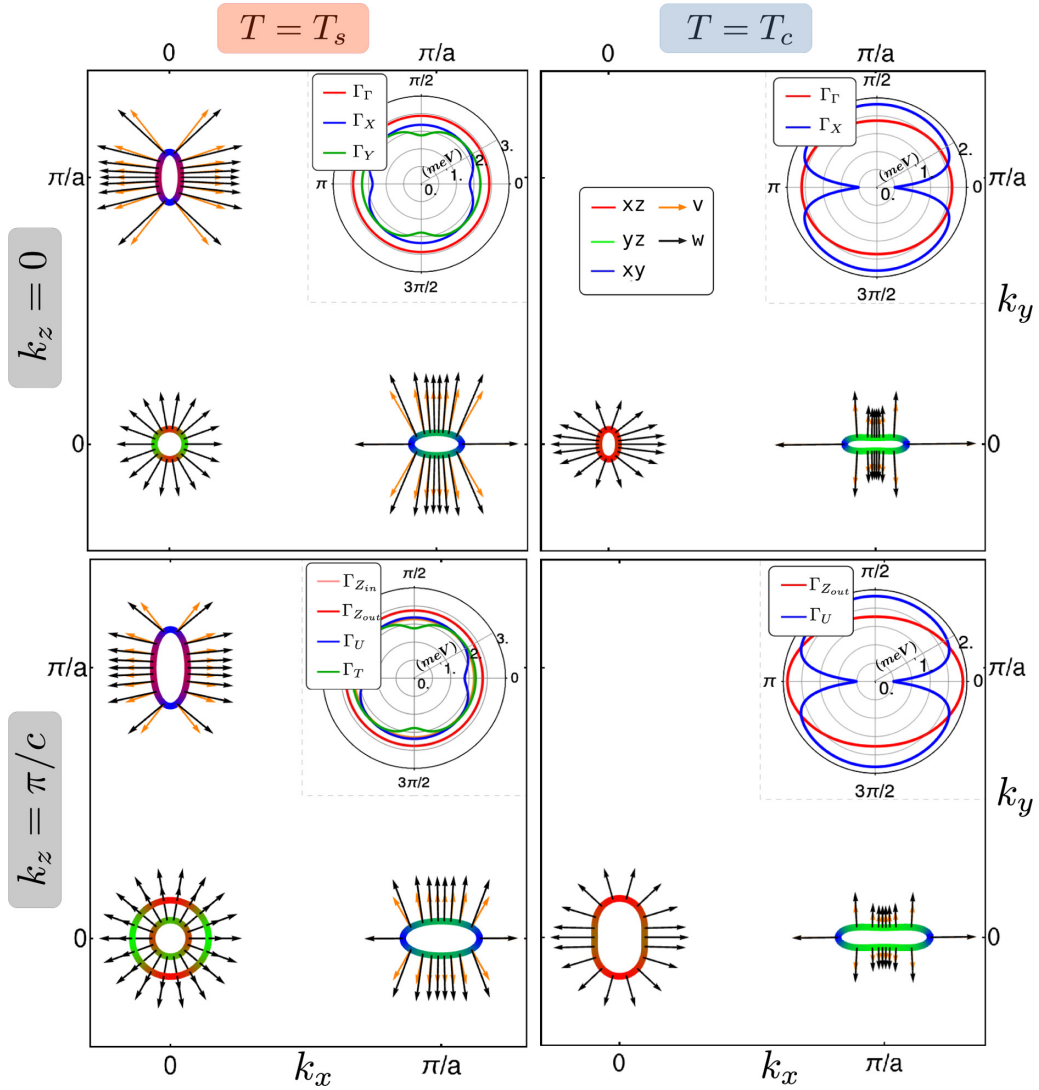
FIG. 2. Fermi pockets, velocities and rates in the 1-Fe BZ. BZ cut at $k_z = 0$ (top row) and at $k_z = \pi/c$ (bottom row); at the nematic phase transition $T = T_s$ (left column) and at the superconducting phase transition $T = T_c$ (right column), that represents a lower bound for our calculations. The pockets are RGB colored according to their orbital weight. The arrows refer to the bare Fermi velocities $\mathbf{v}$ (orange line) and to the dressed ones $\mathbf{w}$ (black lines), multiplied by an overall common constant for all pockets for visualization purposes. In the insets, we show the quasiparticle rates as a function of the polar-angle coordinate along the Fermi pockets.

approximation cannot be made and the computation of $\mathbf{w}$ has to be tackled without simplifications. In Ref. [51] we recently found an explicit solution (see Appendix B), which is semianalytical in the sense that it requires much less numerical computation than what would be required from a naïve solution strategy. As a result, the renormalized velocities can be presented as the sum of two contributions:

$$\mathbf{w}_{\mathbf{k},b} = \mathbf{v}_{\mathbf{k},b} + \kappa \sum_{mnm'n'}^{N_b} e_{\mathbf{k},b}^{m*} e_{\mathbf{k},b}^{n} \big[\big(\mathbb{1} - K_{\varepsilon_{\mathbf{k}}}\big)^{-1} \big]_{nn'}^{mm'} \mathbf{F}_{\varepsilon_{\mathbf{k}}}^{m'n'}, \quad (7)$$

where κ sets the intensity of the impurity on the scattering, K is a $N_b \times N_b \times N_b \times N_b$ tensor describing the scattering among the eigenstates at the orbital level, $\mathbf{F}$ is a vector of $N_b \times N_b$ matrices where velocity and orbital content of the eigenstates are mixed (see Appendix B for their definitions). The second term of the equation represents the equivalent

of what are usually named vertex corrections within the diagrammatic Kubo approach [52]. Finally, the conductivity is obtained as the linear response of the current density to the external field and inherits the two-contributions structure of the renormalized velocities. The first contribution is the bare one while the second is the correction due to the impurity scattering. They are explicitly given by:

$$\sigma_{ij} = \sigma_{ij}^{\text{bare}} + \sigma_{ij}^{\text{corr}}$$

$$\sigma_{ij}^{\text{bare}} = \frac{e^2}{\mathcal{V}} \int_{\varepsilon} (-\partial_{\varepsilon} f_{\varepsilon}) \sum_{b,\mathbf{k}(\varepsilon)} \left(v^i \frac{\tau}{|v|} v^j \right)_{\mathbf{k},b}$$

$$\sigma_{ij}^{\text{corr}} = \frac{e^2 \kappa}{\mathcal{V}} \int_{\varepsilon} (-\partial_{\varepsilon} f_{\varepsilon})$$

$$\times \sum_{mn,m'n'} \big(F_{\varepsilon}^{i*} \big)^{mn} (\mathbb{1} - K_{\varepsilon})^{-1}_{mn,m'n'} \big(F_{\varepsilon}^{j} \big)^{m'n'} \quad (8)$$

with e the electronic charge and $\mathcal{V}$ the sample volume. With these formulas at hand we can account for the effects of the temperature-dependent parameters Φ_T^h, Φ_T^e, Φ_T^{xy}, and $\Delta\epsilon_T^{xy}$ on all the relevant quantities, i.e., the band structure, which enters via the bare velocities $\mathbf{v}_{\mathbf{k},b}$, the impurity scattering, which affects both the quasiparticle scattering rates $\Gamma_{\mathbf{k},b}$ and the renormalized velocities $\mathbf{w}_{\mathbf{k},b}$ of each pocket, and the conductivity.

IV. DC-CONDUCTIVITY ANISOTROPY IN NEMATIC FeSe

A. Scattering rates and renormalized velocities

To better understand the different contributions to the dc conductivity of nematic FeSe we show in Fig. 2 the velocities $\mathbf{v}$, the dressed velocities $\mathbf{w}$ and the quasiparticle rates Γ for each pocket at energy $\varepsilon = \mu_T$ for $T = T_s, T_c$. To ease the reading, in the following discussion we will refer only to the pockets at $k_z = 0$, but the reader has to keep in mind that exactly the same physics takes place for the corresponding pockets at $k_z = \pi/c$. At the nematic transition the pockets at X and Y coincide up to a C_4 rotation and their dressed velocities are quite different from the bare ones. It is noticeable from the figure, however, that there are no velocity corrections along one direction, namely $\mathbf{w}_{x(y)} \equiv \mathbf{v}_{x(y))}$ for the pocket $X(Y)$. At the Γ pocket, corrections are absent at all momenta, i.e., $\mathbf{w} \equiv \mathbf{v}$ for all states. These findings can be understood by explicit analysis of the Hamiltonian symmetries, as we detail in Appendix A. As far as the scattering rates are concerned, they are rather isotropic even in the electronic pockets, despite the pronounced ellipticity. We stress that the rates Γ are small ($\sim 1\,meV$) in comparison with the bands energies ($\sim 100\,$meV), which confirms the validity of the Born approximation (to know how we determined the parameter κ, see Sec. IV B).

By lowering the temperature, the Y pocket sinks below the Fermi energy and the other pockets get sensibly warped. Despite these deformations, we find that a simplified approach using relaxation time approximation [51,52] would work even better at low temperatures, since $\mathbf{w}$ and $\mathbf{v}$ are almost parallel in all pockets. As is clear from the figure, the dressing of velocities of the $X(Y)$ pocket tends to enhance $y(x)$ conductivity. At the same time, once the Y pocket has disappeared the scattering rate on the remaining X pocket becomes strongly anisotropic, with cold spots appearing in the x direction. This effect can be ascribed to the lack of xy orbitals in the other pockets at the Fermi surface, that results in a suppression of scattering events in the X pocket at momenta where the xy orbital component is the largest. As we will see below, the presence of cold spots leads to an increase of bare conductivity along x, in disagreement with the experiments. However, the effect of the velocities renormalization is quantitatively larger than that of the scattering-rate suppression, and overall the X pocket has enhanced conduction along y. Such physics may be different when a different kind of disorder is considered. For instance, with the GUE disorder considered in Appendix C, the scattering rates turn out to be homogeneous across the BZ (there are no cold or hot spots) and there is no velocities renormalization. Still, the observed resistivity anisotropy has the right sign because in this case the bare-band velocities
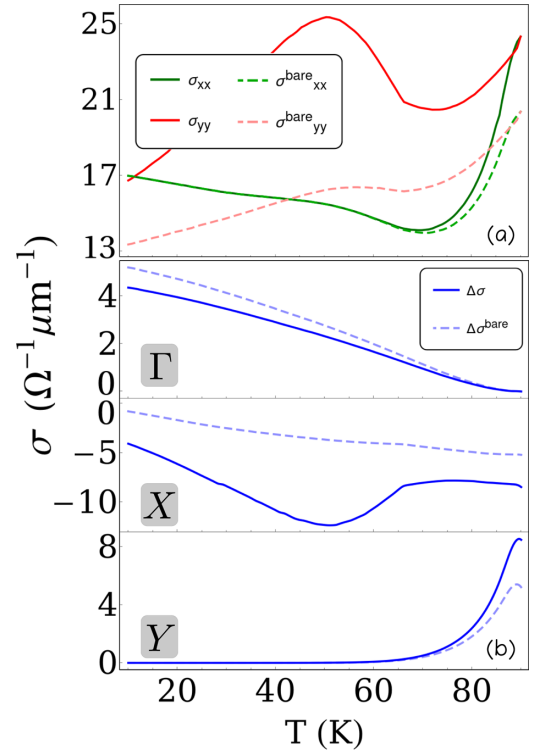

FIG. 3. Diagonal dc conductivities as a function of temperature. (a) dc conductivity along x and y, with (solid lines) and without (dashed lines) corrections, computed from Eq. (8). (b) contributions to the dc conductivity anisotropy $\Delta\sigma = \sigma_{xx} - \sigma_{yy}$ from all pockets grouped by their locations Γ, X and Y in the BZ (the contributions from the Z, U, T pockets are summed to those ones, respectively).

alone (which stay the same as those in Fig. 2) suffice to give a higher y conductivity in the nematic phase.

B. dc conductivity and resistivity anisotropy

In Fig. 3(a) we show the dc conductivities along x and y. As expected from the previous considerations and the theory [51], $s_{xx} < s_{yy}$ and vertex corrections provide only positive contributions as one can see by comparing s with s^{bare}. Moreover, by lowering the temperature the corrections vanish at about $65K$ for the x direction as $F^x \simeq 0$ due to the sinking of the Y pocket and a major kink appears. The different contributions of the various pockets grouped with respect to their location in the BZ are shown in Fig. 3(b). We must mention that the contributions from pockets lying above or below the Fermi energy and within the temperature broadening are conspicuous but qualitatively irrelevant. So, to ease the discussion, here we do not comment over their scattering rates, their velocities profiles, and their contribution to the conductivities and focus only on the pockets at the Fermi level. At high temperatures the largest contributions to $\Delta\sigma \equiv \sigma_{xx} - \sigma_{yy}$ come from the X and Y pockets, the Γ one being almost irrelevant (due to high scattering rates and small velocities). Decreasing the temperature the Y contribution vanishes, leaving the ground to the negative X contribution. Finally, at small temperatures the Γ contribution to $\Delta\sigma$ increases, eventually beating the X one. The vertex corrections of the X pocket are at least two orders
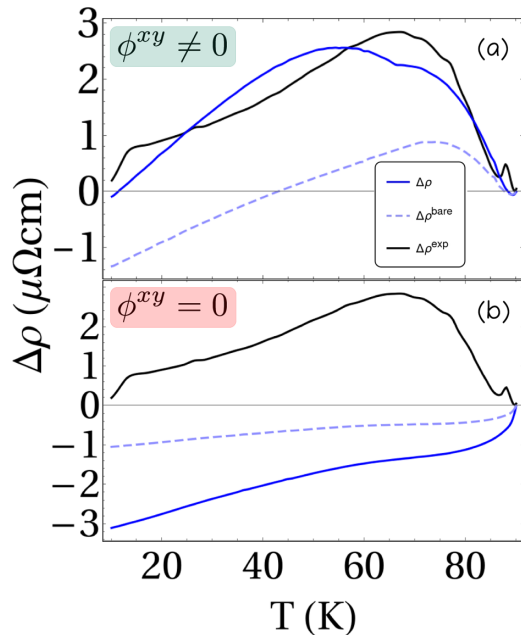
FIG. 4. Resistivity anisotropy as a function of temperature. (a) Resistivity anisotropy obtained by including ($\Delta\rho$, blue solid line) or not ($\Delta\rho^{\text{bare}}$, blue dashed line) the velocities renormalization. We also show for comparison the experimental data ($\Delta\rho^{\text{exp}}$, black line) of the dc resistivity anisotropy taken from Ref. [36]. (b) Same as (a) but without inclusion of the xy nematic parameters Φ^{xy} and $\Delta\epsilon^{xy}$.

of magnitude bigger than the bare conductivity and make them crucial for the match with experiment. Indeed, while $\Delta\sigma_X^{\text{bare}}$ rapidly approaches zero, due mainly to the cold-spot effect mentioned earlier, the full $\Delta\sigma_X$ remains negative and compensates the positive $\Delta\sigma_\Gamma$ from the hole pocket.

In Fig. 4(a) we show the resistivity anisotropy $\Delta\rho = 1/s_{xx} - 1/s_{yy}$ and compare it with the experimental data of Ref. [36]. The only fitting parameter is the overall scale of the resistivity controlled by the factor $n_I v_I^2$ inside κ [see Eq. (B1)]. Since the volume of the sample of Ref. [36] can be estimated to be roughly $1\,\text{mm}^2 \times 80\,\mu\text{m}$, assuming $v_I = 50\,\text{meV}$ we find the impurity concentration equals 10%. The value is quite high considered that the experimental sample is supposed to be clean, according to the authors. However, we note that on the one hand the value has a big margin of error and on the other it is already small enough to allow for the Born approximation to be reasonably good. The match between theory and experiments is very good, despite a change of sign of the theoretical curve $\Delta\rho$ at low temperature, that must be, however, taken with care considering that we are not including precursor effects expected before than the superconducting transition at T_c. The figure shows also the mentioned importance of the vertex-correction term. Clearly $\Delta\rho^{\text{bare}}$ does not match the experiments, to the extent that it even changes sign at quite high temperatures $T \sim 40\,\text{K}$; notice that a different κ fitting parameter may improve the match only at high temperature, making the situation worse at lower ones. We may conclude that vertex corrections (finite along y and quenched along x) coming from the multiorbital nature of the system are crucial in opposing the bare-bands conductivity tendency to favor negative values of $\Delta\rho$.

It is also interesting to check how different nematic scenarios can affect the final results for the resistivity anisotropy. In particular, it is worth computing $\Delta\rho$ when only the xz/yz nematic order parameter (1) is introduced. Numerical details and band parameters for this case are discussed in Appendix D. In Fig. 4(b) we show the final results, and one clearly sees that the resistivity anisotropy has the wrong sign and cannot describe the experimental observations. The main reason is that when $\Phi^{xy} = 0$ the Y pocket survives below T_s and it even increases in size by lowering the temperature. This has the twofold effect of suppressing the cold spots at the X pocket and, more importantly, to leave active the large conduction along x due to the Y pocket, where both the bare and renormalized velocities are quantitatively larger than in the X pocket due to the larger size. As a consequence, vertex corrections in this case reinforce the negative trend of the bare resistivity anisotropy, in stark contrast with the experiments. In the Appendix C we show a check that our theoretical model fits the experimental data also when different kinds of impurity disorder are considered.

V. DISCUSSION AND CONCLUSIONS

When comparing the results in Figs. 4(a) and 4(b) one sees that within the present approach the physical mechanism behind the anisotropy of the transport in FeSe originates from a strong reduction of both the xy and xz orbital components at the Fermi surface, due to the fact that the Y pocket sinks down the Fermi level. Indeed, even though the disappearing of the Y pocket induces a cold-spot effect, with a strong increase of the relaxation time at the electron X pocket for transport along x, such an effect is completely overcompensated by the velocities renormalization. As a consequence, in analogy with previous findings in the context of inelastic scattering [46], the usual interpretation in terms of hot and cold spot should be taken with care, since vertex corrections actually change the final result, and their inclusion becomes crucial to account for the experimental observations. In contrast, when the Φ^{xy} nematic order parameter is absent, as in Fig. 4(b), vertex corrections reinforce the tendency of the bare conductivity anisotropy to favor transport along y, leading to an overall negative $\Delta\rho$ below T_s. Notice that in this view both the inclusion of the xy nematic order parameter and the inclusion of the velocities renormalization into the dc conductivity are crucial ingredients to reproduce the resistivity anisotropy observed in FeSe.

On a wider perspective, our results suggest that for FeSe the emergence of a xy order parameter (2) not only explains the disappearance of the Y pocket in ARPES measurements [21], a surface probe, but it is also crucial to account for the resistivity anisotropy, a bulk probe. It is worth stressing that our calculations cannot reproduce the typical linear increase of the resistivity as a function of temperature [36], which is due to inelastic scattering processes that are dominant in the whole temperature range considered. However, at very low temperature (and in the absence of the superconducting transition at T_c) inelastic scattering would be suppressed, and the elastic one due to impurities would become dominant. In this respect we notice that the corresponding extrapolated value s_0^{imp} of the experimental conductivity approximately coincides
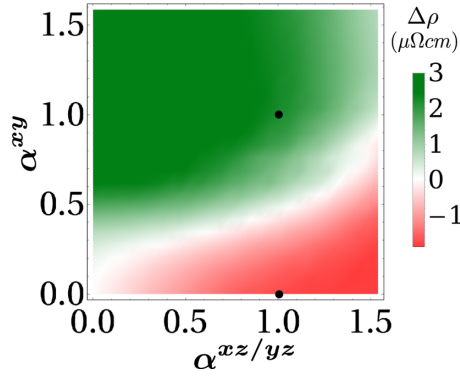
FIG. 5. Resistivity anisotropy at $T = 50K$ for different values of the nematic order parameters. For the definition of the scaling constants $\alpha_{xz/yz}, \alpha_{xy}$ see the text. The chemical potential at each value of the parameters is determined self-consistently such that the electron density is the same across all values. The top and bottom black dots mark the parameter values considered in Figs. 4(a) and 4(b), respectively.

with the average of the conductivities along x and y computed within our model. Since this is also the parameter setting the overall scale of the resistivity anisotropy, the present result reinforces the possibility that resistivity anisotropy can be ascribed mainly to elastic processes. Such a conclusion is further supported by various experiments carried out in annealed samples of certain electron-doped 122 compounds, where the anisotropy is suppressed with annealing [38,39]. Despite the fact that electron correlations in FeSe seem to be the strongest among all Fe-based superconductors [3], the fact that the parameters used reproduce both the measured Fermi surface and the extrapolated low-temperature resistivity suggests that the anisotropy could be probably linked to elastic impurity scattering also in this case.

To make a closer connection to the case of most 122 compounds, we report in Fig. 5 the resistivity anisotropy for a fixed disorder level as a function of the strength of the nematic order parameters (1) and (2). To show this effect in a compact way, we group them in two independent sets $(\Phi^h, \Phi^e)_T = \alpha_{xz/yz}\sqrt{1 - \frac{T-T_c}{T_s}}(\Phi^h, \Phi^e)_{T_c}$ and $(\Phi^{xy}, \Delta\epsilon^{xy})_T = \alpha_{xy}\sqrt{1 - \frac{T-T_c}{T_s}}(\Phi^{xy}, \Delta\epsilon^{xy})_{T_c}$, governed by the parameters $\alpha_{xz/yz}, \alpha_{xy}$. At $\alpha_{xz/yz} = \alpha_{xy} = 1$ the resistivity anisotropy is the one shown before in Fig. 4. In Fig. 5 we plot $\Delta\rho$ as an intensity plot at generic values of $\alpha_{xz/yz}, \alpha_{xy}$ but fixed $T = 50$ K. All the red region corresponds to the case $\Delta\rho < 0$, as measured in 122 systems [29–34], and it still persists for a moderate value of the xy order parameter, showing that in principle one cannot exclude a moderate xy nematicity also in 122 compounds. We remind the reader, however, that the comparison with the 122 case is still done within a four-pocket model, that does not necessarily apply to the whole 122 class. For instance in $BaFe_2Se_2$ a large hole pocket at Γ of d_{xy} character is present. Even though this hole pocket is regarded to be an incoherent one and thus not very influential in the transport [61], in principle one should check whether the inclusion of such an incoherent xy pocket change the present results. An other interesting feature happens in

K-doped 122 compounds, where the resistivity anisotropy changes sign at moderate doping [35] from negative to positive. Such change cannot be captured by our model simply by changing the intensity of the disorder, which only changes the intensity of the resistivity. As a consequence, within our picture we can understand this result as a change of nematic ordering in the various orbitals. In particular, the experimental findings are compatible with a progressive weakening of the xz/yz nematicity as compared to the xy one, possibly due to a weakening of spin-nematic xz/yz fluctuations within a OSSF model due to progressive suppression of quasinesting conditions among holelike and electronlike pockets with doping. An increasing of $\alpha^{xy}/\alpha^{xz/yz}$ in Fig. 5 would imply that the systems starts at one point in the red region for the undoped compound and then as hole doping increases it moves in the green one. We finally mention that the different sign of the anisotropy between 122 compounds and FeSe has been explained before [50] by means of a simplified but fully quantum approach that was including spin fluctuations instead of impurity scattering. However, the purpose of that paper was not to compare quantitatively with the experimental data, and since the orbital model Hamiltonian was not fitting the ARPES measurements the results had a certain degree of parameter dependency. By contrast, our model is robust against parameters change (see Fig. 5), against the disorder model (see Appendix C), and fits the experiment at a reasonable quantitative level. Clearly a combination of the two approaches may provide a more complete view on the problem.

In summary, we computed the resistivity anisotropy in the nematic phase of FeSe due to elastic impurity scattering. We showed that when disorder is introduced at the level of the microscopic orbital model the multiorbital structure induces nontrivial effects on the transport properties, with the emergence of velocity-renormalization effects at the level of the Boltzmann transport equation. By taking advantage of our recently derived semianalytical solution of the problem [51], we computed the resistivity anisotropy in the nematic phase, comparing the results for different nematic scenarios. We find that to reproduce the experimentally observed resistivity anisotropy of FeSe it is crucial not only to account for the full solution of Boltzmann equation, but also to add, along with the xz/yz nematic order parameter, the xy nematic order recently proposed in Ref. [28]. The latter plays indeed a crucial role in order to reverse sign of the full conductivity with respect to the bare one, due only to the Fermi-surface deformation below T_s. As the xy nematic order parameter is suppressed the full resistivity anisotropy has instead the same sign of the bare one, and one recovers the experimental observations in 122 compounds. Our results highlight how the additional xy nematic order has a strong impact on bulk transport properties of FeSe, besides the direct effect on the Fermi-surface topology, with the disappearing [21,28] of the Y pocket below T_s. To further test the interplay among impurity scattering and nematicity it would be interesting to explore, e.g., how transport evolves under uniaxial strain [62], and/or in the presence of a magnetic field. Indeed, the marked anomaly of the Hall coefficient of FeSe upon entering the nematic phase rapidly disappears as nematicity softens upon, e.g., S doping [63],

clearly suggesting a deep connection with nematic order. The relevance of velocity renormalization for the Hall effect in compensated semimetals such as pnictides has been already emphasized in previous work accounting for interband interactions due to inelastic effects [64]. It would be then very interesting to investigate if also impurity scattering within a multiorbital model has a similar effect, and the role played by different nematic scenarios. Finally, the microscopic justification for the xy nematicity itself remains an open challenge, with crucial implications for all families of pnictides.

APPENDIX A: HAMILTONIAN PARAMETERS AND SYMMETRIES

All terms of the full effective Hamiltonian, Eq. (3) in the main text, are defined for $k_z = 0$ as:

$$H^{0\,\Gamma}(\mathbf{k}) = \left[\epsilon^h - \frac{k^2}{2m_h}\right]\tau_0 \otimes \sigma_0 - \left[\frac{r}{2}\left(k_x^2 - k_y^2\right)\right]\tau_3 \otimes \sigma_0 + rk_xk_y\tau_1 \otimes \sigma_0 + \frac{\lambda_{\mathrm{SOC}}^h}{2}\tau_2 \otimes \sigma_3,$$

$$H_T^{\Phi\,\Gamma}(\mathbf{k}) = \Phi_T^h\,\tau_3 \otimes \sigma_0,$$

$$H^{0\,X/Y}(\mathbf{k}) = \left[\frac{k^2}{2}\left(\frac{1}{2m_1} + \frac{1}{2m_3}\right) - \frac{1}{2}(\epsilon^{e1} + \epsilon^{e2}) \mp \frac{1}{4}(a_1 + a_3)\left(k_x^2 - k_y^2\right)\right]\tau_0 \otimes s_0,$$

$$+ \left[\frac{k^2}{2}\left(\frac{1}{2m_1} - \frac{1}{2m_3}\right) - \frac{1}{2}(\epsilon^{e1} - \epsilon^{e2}) \mp \frac{1}{4}(a_1 - a_3)\left(k_x^2 - k_y^2\right)\right]\tau_3 \otimes s_0,$$

$$+ v_{X/Y}(\mathbf{k})\tau_2 \otimes s_0,$$

$$H_T^{\Phi\,X/Y} = \left(\frac{\Delta\epsilon_T^{xy}}{2} \pm \frac{\Phi_T^e - \Phi_T^{xy}}{2}\right)\tau_0 \otimes s_0 - \left(\frac{\Delta\epsilon_T^{xy}}{2} \mp \frac{\Phi_T^e + \Phi_T^{xy}}{2}\right)\tau_3 \otimes s_0, \tag{A1}$$

where the Pauli matrices τ, s act on the orbital and spin spaces, respectively, and the slash in the label X/Y is linked with $\pm$ symbols; we denote[1]

$$v_X(\mathbf{k}) = \sqrt{2}vk_y + \frac{p_1}{\sqrt{2}}\left(k_y^3 + 3k_yk_x^2\right) - \frac{p_2}{\sqrt{2}}k_y\left(k_x^2 - k_y^2\right)$$

$$v_Y(\mathbf{k}) = \sqrt{2}vk_x + \frac{p_1}{\sqrt{2}}\left(k_x^3 + 3k_xk_y^2\right) - \frac{p_2}{\sqrt{2}}k_x\left(k_y^2 - k_x^2\right). \tag{A2}$$

At $k_z = \pi/c$ the Hamiltonian terms have the same formal expressions but different parameter values. The chemical potential μ_T is computed so to ensure the same average number of electrons at all temperatures taking as a reference value the one at 10 K given in Ref. [28]. All values of the parameters appearing in the Hamiltonian are taken from the same reference and are listed in Table I. We use the 1-Fe lattice constant $a = 2.61\,\text{Å}$ and $c = 5.52\,\text{Å}$ (the b lattice constant differs from a in the nematic phase only by a tiny fraction that we neglect) [65]. Notice that the $\Delta\epsilon^{xy}$ and Φ^{xy} have the same effects on the xy orbital at the Y point. However, at the X one they act distructively thus being almost ineffective on this pocket. In principle the X, Y, U, T pockets experience a tiny spin-orbit coupling $\lambda_{SOC}^e = 4$ meV that we neglect to simplify the numerics. The approximation involves a change in the actual Fermi surface removing the anticrossing between spin bands. Even though this change is relevant for Hall measurements,

it is not for diagonal conductances due to the small energy magnitude of the spin-orbit coupling as compared to that of other parameters.

The Hamiltonian has the following symmetries [53] (the symmetries at Z, U, T have the same form of those at Γ, X, Y shown here):

TABLE I. Hamiltonian parameters list. Effective Hamiltonian parameters for each sector of the 1-Fe BZ, obtained by fitting ARPES data at $T = T_c$. (Adapted from Ref. [28]).

	Γ	Z	
ϵ^h	-8	12	meV
$\frac{1}{2m_h}$	4730	1998.4	meV Å^2
r	4664	1970.54	meV Å^2
Φ_T^h	15	15	meV
λ_{SOC}^h	23	23	meV
	X, Y	U, T	
ϵ^{e1}	30.6	30.6	meV
ϵ^{e2}	48.6	48.6	meV
$\frac{1}{2m_1}$	10.2060	4.54	meV Å^2
$\frac{1}{2m_3}$	1355.9	602.64	meV Å^2
α_1	991.44	440.64	meVÅ^2
α_3	-2937.9	-1305.7	meV Å^2
v	-329.4	-219.6	meV Å
p_{z_1}	-2700.9	-800.27	meV Å^3
p_{z_2}	-229.7	-68.06	meV Å^3
Φ_T^e	-26	-26	meV
Φ_T^{xy}	45	45	meV
$\Delta\epsilon_T^{xy}$	40	40	meV

---

[1]We note that the sign in front of the parameter p_2 in the definition of v_y differs from that in Ref. [25]. However, with our choice v_y respects all spatial symmetries of the system in agreement with the analysis of Ref. [53].

(i) x/y-axis reflection symmetry at X/Y and inversion symmetry at Γ, i.e., $H^{(X)}(k_x, k_y) = H^{(X)}(-k_x, k_y)$, $H^{(Y)}(k_x, k_y) = H^{(Y)}(k_x, -k_y)$ and $H^{(\Gamma)}(k_x, k_y) = H^{(\Gamma)}(-k_x, -k_y)$ (here, the origins of the momenta are the X, Y, and Γ points, respectively);

(ii) $H^{(X)}(k_x, k_y) = \tau_3 H^{(X)}(k_x, -k_y)\tau_3$ and $H^{(Y)}(k_x, k_y) = \tau_3 H^{(Y)}(-k_x, k_y)\tau_3$ where the Pauli matrix act on the orbital degree of freedom;

(iii) Time-reversal symmetry $H_{\mathbf{k}} = s_2(H_{-\mathbf{k}})^* s_2$, where the Pauli matrix acts on the spin degree of freedom.

(iv) Spin-rotation invariance at X and Y, due to the neglect of spin-orbit coupling (see Appendix A), while only conservation of the z component of the spin at Γ.

Notice that these symmetries imply that the up and down spin sectors are totally decoupled and degenerate.

The peculiar properties of **w** discussed in Sec. IV of the main paper stem directly from the symmetry of the Hamiltonian, in the following way. By symmetries (i) $F^{x(y)}$ gets contributions only from the pocket $Y(X)$. The pocket Γ do not contribute to **F** at all. Moreover $F^{x(y)}$ is strictly an off-diagonal matrix due to symmetries (ii) and the simultaneous invariance of $\tau_{Y(X)}$ and sign reversal of $v_{Y(X)}^{x(y)}$ under $(k_x, k_y) \rightarrow (k_x, -k_y)$ $[(k_x, k_y) \rightarrow (-k_x, k_y)]$. Following a similar reasoning the K tensor, viewed as a matrix indexed with two-pockets labels both per raw and per columns, is actually a block matrix. In particular the 2×2 block concerning the xy-xz and xz-xy elements and the one concerning the xy-yz and yz-xy ones constitute two independent blocks that are uncoupled to the other elements. This block structure carries over to the tensor $(\mathbb{1} - K)^{-1}$. Thus, the property $w_X^x = v_X^x$ follows from the absence of match of $(\mathbb{1} - K)^{-1}F^x$, having only xy-xz and xz-xy elements, and the projector onto the eigenstates of X, having no components involving the orbital xz. The properties of **w** for the other pockets follow from similar arguments. It is quite remarkable how the general properties of the vertex corrections can be drawn from the analysis of K and **F** despite the complexity of the system.

APPENDIX B: SEMIANALYTICAL SOLUTION OF THE BOLTZMANN EQUATION

The collision integral kernel used in the Boltzmann equation (5) is elastic and comes from a disorder term in the Hamiltonian, which is diagonal in the band index. Such kind of disorder is arguably the simplest one may consider and is the one that is usually used in calculations. Interestingly enough, the collision integral kernel in not diagonal in the band index:

$$Q_{\mathbf{k}\mathbf{k}'}^{bb'} = \kappa |\mathbf{e}_{\mathbf{k},b} \cdot \mathbf{e}_{\mathbf{k}',b'}|^2 \, \delta(\varepsilon_{\mathbf{k},b} - \varepsilon_{\mathbf{k}',b'}), \qquad (B1)$$

where $\mathbf{e}_{\mathbf{k},\mathbf{b}}$ represents an eigenvector of the multiorbital Hamiltonian, $\kappa = 2\pi n_{imp} v_{imp}^2 a^2 c / \mathcal{V}$ (n_{imp} is the impurity concentration and v_{imp} their potential energy) and $\varepsilon_{\mathbf{k},b}$ is the electron energy. The Boltzmann equation at zeroth order in **E** is trivially solved by the Fermi function $f(\varepsilon_{\mathbf{k}}^b)$. At first order the equation can be written as an integral equation for $\mathbf{w}_{\mathbf{k},b}$:

$$\sum_{\mathbf{k}',b'} \left(\delta_{\mathbf{k}\mathbf{k}'}\delta_{bb'} - Q_{\mathbf{k}\mathbf{k}'}^{bb'} \tau_{\mathbf{k}'}^{b'} \right) \mathbf{w}_{\mathbf{k}'}^b = \mathbf{v}_{\mathbf{k}}^b. \qquad (B2)$$

The numerical solution of Eq. (B2) is rather demanding, since it requires us to invert the large matrix $1 - Q\tau$ in the grouped indexes $(\mathbf{k}b)$ and $(\mathbf{k}'b')$ in the left-hand side of the equation (B2). In Ref. [51] we recently proposed a semianalytical solution to this problem. More specifically, we showed that thanks to the energy conservation implicit in the collision-integral kernel (B1) the matrix $1 - Q\tau$ becomes block diagonal when the **k** vectors are ordered in groups belonging to the same energy shell. These blocks are finite rank, allowing one to reduce the problem to the inversion of a small matrix whose size N_b^2 is set by number of orbitals. The solution is given in Eq. (7). As one can see, we reduced the complex problem of inverting the integral equation (B2) to that of inverting the tensor $\mathbb{1} - K$, which, together with the matrix F, can be readily computed once the original multiorbital model (3) has been diagonalized.

The tensors K and **F** are defined as

$$(K_\varepsilon)_{mn,m'n'} = \kappa \sum_{b,\mathbf{k}(\varepsilon)} (e^m e^{n*} e^{m'*} e^{n'} \, \tau)_{\mathbf{k},b} \qquad (B3)$$

and

$$\mathbf{F}_\varepsilon^{mn} = \sum_{b,\mathbf{k}(\varepsilon)} (e^m e^{n*} \, \tau \, \mathbf{v})_{\mathbf{k},b}, \qquad (B4)$$

where in both expressions we use the shorthand notation (valid in the thermodynamic limit) $\sum_{b,\mathbf{k}(\varepsilon)} = \mathcal{V} \int \frac{d^3\mathbf{k}}{(2\pi)^3} \delta(\varepsilon_{\mathbf{k},b} - \varepsilon)$. The full current density is defined as usual: $\mathbf{J} = -\frac{e}{\mathcal{V}} \sum_{\mathbf{k},b} (\mathbf{v}\rho)_{\mathbf{k},b} = \frac{e^2}{\mathcal{V}} \sum_{\mathbf{k},b} \mathbf{v}_{\mathbf{k},b} \tau_{\mathbf{k},b} (\mathbf{w}_{\mathbf{k},b} \cdot \mathbf{E})(-\partial_{\varepsilon_{\mathbf{k}}^b} f_{\varepsilon_{\mathbf{k}}^b})$ and is linear in **E**. By inserting the result (7) into this expression, the conductivity matrix of Eq. (8) is obtained from the relation $\mathbf{J} = \sigma \mathbf{E}$.

APPENDIX C: NEMATIC FeSe WITH GOE AND GUE DISORDER

Does the correct characterization of the experimentally measured resistivity anisotropy with the model described in Sec. III rely on the specific type of disorder chosen? In this Appendix we show numerical results obtained by using different models of disorder and verify the robustness of our findings. In particular, we explore the possibility that the local impurities do not only shift the local chemical potential but may couple differently the various electronic orbitals and in a random way, so that a statistical approach would be feasible. Namely we take each impurity Hamiltonian matrix to be drawn from a Gaussian unitary or orthogonal ensemble (GUE or GOE), instead of being simple diagonal matrices of magnitude v_{imp} as in the main text. The theory for such kind of disorder ensembles is slightly more complicated than the one presented in Sec. III. The band structure and the bare velocities stay the same as before, but Eqs. (9)–(11) are different resulting in different rates and dressed velocities; we refer to Ref. [51] for the general formulas. In the case of FeSe, the GUE may be employed to describe disorder from impurities that produce nonvanishing microscopic magnetic fields (that vanish macroscopically) that couple the spins and break the time-reversal symmetry of H_{eff}. Conversely, the GOE may be employed to describe nonmagnetic disorder,
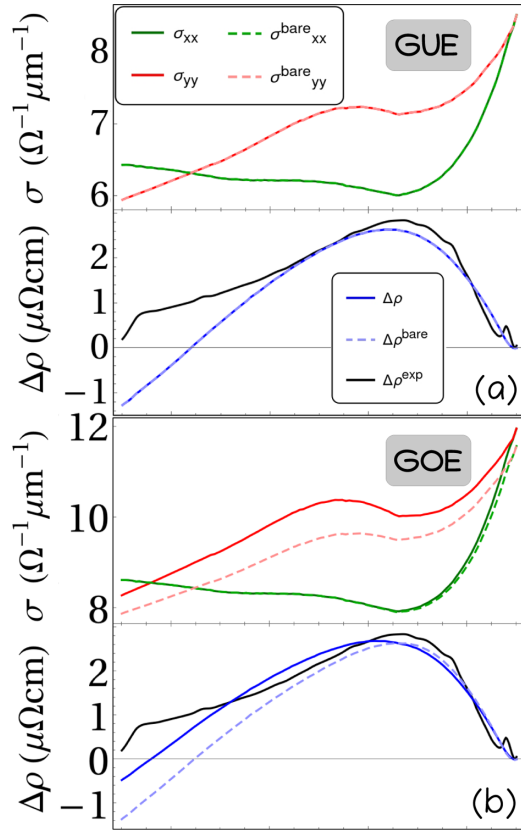
FIG. 6. Diagonal dc conductivities with different disorder types. Conductivities along x and y using the same labels as in Figs. 3 and 4, assuming GUE (top) or GOE (bottom) disorder.

which is diagonal in the spin space and commutes with the spinless time-reversal operator $\hat{K}$ (complex conjugation). The results for the conductivity and the resistivity are shown in Fig. 6. The fits are qualitatively similar to that of Figs. 3(a) and 4(a), the GUE-disordered system performing worse, the GOE one performing better. Notice how the GUE disorder induces no velocities renormalizations (dashed curves coincide exactly with the darker ones), but in this case $\Delta\rho^{\mathrm{bare}}$ has the same sign of the experiments in most of the temperature range. This happens because there is no notion of hot and cold spots for this ensemble as there is a unique (isotropic) scattering rate for all states, such as in single-band models. Thus, only the bare velocities of the pockets matter, which clearly favor the right sign due to the sinking of the Y pocket. The GOE disorder produces instead positive corrections, as expected from the theoretical discussion of Ref. [51] and also in this case such corrections are relevant in order to achieve a better agreement with experiments. These examples underline the fact that vertex corrections need not be an essential feature of the system that will describe the experiment but they must be included whenever they are finite. Finally, we remark that the absolute magnitude of the conductivities (not shown) in these cases is much smaller than in the other one, even though one tunes κ in order to have the correct magnitude of the resistivity anisotropy. It is surprising because one could expect that the fitting parameter, that tunes separately
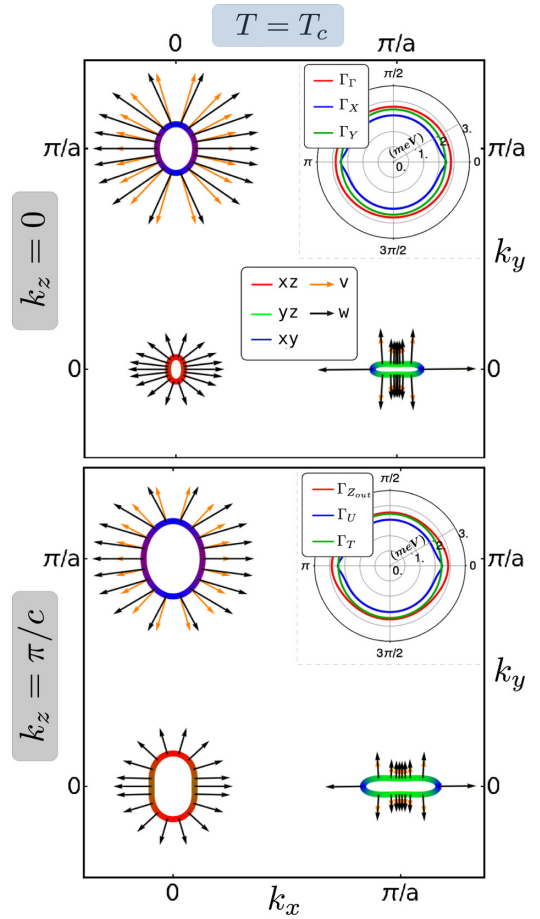

FIG. 7. Fermi pockets, velocities, and rates in the 1-Fe BZ without xy nematic parameters. Same as Fig. 2, right column, but setting $\Phi^{xy} = \Delta\epsilon^{xy} = 0$.

for each disorder ensembles the matching of the resistivity anisotropy, would also create match among (the magnitudes of) the conductivities. This, however, is unlikely to happen, since the fitting parameter should compensate at the same time for both higher rates (roughly twice with these ensembles due to the higher number of disorder degrees of freedom) and an overall smaller relative difference between the conductivities along the x and y directions. We may conclude that the match between theory and experiment is quite robust against changes of the disorder type.

APPENDIX D: DC ANISOTROPY IN THE ABSENCE OF xy NEMATICITY

To have an idea of the physics in the red region of Fig. 5, in Fig. 7 we show the Fermi surfaces at T_c in the absence of the xy nematic order, i.e., $\alpha^{xy} = 0$ or equivalently $\Phi_T^{xy} \equiv \Delta\varepsilon_T^{xy} \equiv 0$ in the Hamiltonian (A1). In this case the Fermi pockets at Y and T do not vanish, instead they increase in size as the temperature lowered. As a result, the density of states and the velocity profile favor the conductivity along the direction x, determining the negative resistivity anisotropy reported in Fig. 4(b).

[1] Y. Gallais and I. Paul, Charge nematicity and electronic raman scattering in iron-based superconductors, C. R. Phys. **17**, 113 (2016).

[2] A. I. Coldea and M. D. Watson, The key ingredients of the electronic structure of FeSe, Annu. Rev. Condens. Matter Phys. **9**, 125 (2018).

[3] R. M. Fernandes, A. I. Coldea, H. Ding, I. R. Fisher, P. J. Hirschfeld, and G. Kotliar, Iron pnictides and chalcogenides: A new paradigm for superconductivity, Nature (London) **601**, 35 (2022).

[4] R. M. Fernandes, A. V. Chubukov, J. Knolle, I. Eremin, and J. Schmalian, Preemptive nematic order, pseudogap, and orbital order in the iron pnictides, Phys. Rev. B **85**, 024534 (2012).

[5] R. M. Fernandes, A. V. Chubukov, and J. Schmalian, What drives nematic order in iron-based superconductors? Nat. Phys. **10**, 97 (2014).

[6] S. Baek, D. Efremov, J. M. Ok, J. S. Kim, J. van den Brink, and B. Büchner, Orbital-driven nematicity in FeSe, Nat. Mater. **14**, 210 (2015).

[7] Y. Su, H. Liao, and T. Li, The form and origin of orbital ordering in the electronic nematic phase of iron-based superconductors, J. Phys.: Condens. Matter **27**, 105702 (2015).

[8] S. Mukherjee, A. Kreisel, P. J. Hirschfeld, and B. M. Andersen, Model of Electronic Structure and Superconductivity in Orbitally Ordered FeSe, Phys. Rev. Lett. **115**, 026402 (2015).

[9] K. Jiang, J. Hu, H. Ding, and Z. Wang, Interatomic Coulomb interaction and electron nematic bond order in FeSe, Phys. Rev. B **93**, 115138 (2016).

[10] R.-Q. Xing, L. Classen, M. Khodas, and A. V. Chubukov, Competing instabilities, orbital ordering, and splitting of band degeneracies from a parquet renormalization group analysis of a four-pocket model for iron-based superconductors: Application to FeSe, Phys. Rev. B **95**, 085108 (2017).

[11] L. Fanfarillo, A. Cortijo, and B. Valenzuela, Spin-orbital interplay and topology in the nematic phase of iron pnictides, Phys. Rev. B **91**, 214515 (2015).

[12] L. Fanfarillo, J. Mansart, P. Toulemonde, H. Cercellier, P. Le Fèvre, F. Bertran, B. Valenzuela, L. Benfatto, and V. Brouet, Orbital-dependent fermi surface shrinking as a fingerprint of nematicity in FeSe, Phys. Rev. B **94**, 155138 (2016).

[13] L. Fanfarillo, L. Benfatto, and B. Valenzuela, Orbital mismatch boosting nematic instability in iron-based superconductors, Phys. Rev. B **97**, 121109(R) (2018).

[14] P. Zhang, T. Qian, P. Richard, X. P. Wang, H. Miao, B. Q. Lv, B. B. Fu, T. Wolf, C. Meingast, X. X. Wu, Z. Q. Wang, J. P. Hu, and H. Ding, Observation of two distinct d_{xz}/d_{yz} band splittings in FeSe, Phys. Rev. B **91**, 214503 (2015).

[15] Y. Suzuki, T. Shimojima, T. Sonobe, A. Nakamura, M. Sakano, H. Tsuji, J. Omachi, K. Yoshioka, M. Kuwata-Gonokami, T. Watashige, R. Kobayashi, S. Kasahara, T. Shibauchi, Y. Matsuda, Y. Yamakawa, H. Kontani, and K. Ishizaka, Momentum-dependent sign inversion of orbital order in superconducting FeSe, Phys. Rev. B **92**, 205117 (2015).

[16] Y. Zhang, M. Yi, Z.-K. Liu, W. Li, J. J. Lee, R. G. Moore, M. Hashimoto, M. Nakajima, H. Eisaki, S.-K. Mo, Z. Hussain, T. P. Devereaux, Z.-X. Shen, and D. H. Lu, Distinctive orbital anisotropy observed in the nematic state of a FeSe thin film, Phys. Rev. B **94**, 115153 (2016).

[17] M. D. Watson, A. A. Haghighirad, H. Takita, W. Mansuer, H. Iwasawa, E. F. Schwier, A. Ino, and M. Hoesch, Shifts and splittings of the hole bands in the nematic phase of FeSe, J. Phys. Soc. Jpn. **86**, 053703 (2017).

[18] Y. S. Kushnirenko, A. V. Fedorov, E. Haubold, S. Thirupathaiah, T. Wolf, S. Aswartham, I. Morozov, T. K. Kim, B. Büchner, and S. V. Borisenko, Three-dimensional superconducting gap in FeSe from angle-resolved photoemission spectroscopy, Phys. Rev. B **97**, 180501(R) (2018).

[19] M. Yi, H. Pfau, Y. Zhang, Y. He, H. Wu, T. Chen, Z. R. Ye, M. Hashimoto, R. Yu, Q. Si, D.-H. Lee, P. Dai, Z.-X. Shen, D. H. Lu, and R. J. Birgeneau, Nematic Energy Scale and the Missing Electron Pocket in FeSe, Phys. Rev. X **9**, 041049 (2019).

[20] S. S. Huh, J. J. Seo, B. S. Kim, S. H. Cho, J. K. Jung, S. Kim, C. I. Kwon, J. S. Kim, Y. Y. Koh, W. S. Kyung, J. D. Denlinger, Y. H. Kim, B. N. Chae, N. D. Kim, Y. K. Kim, and C. Kim, Absence of Y-pocket in 1-Fe Brillouin zone and reversed orbital occupation imbalance in FeSe, Commun. Phys. **3**, 52 (2020).

[21] L. C. Rhodes, M. Eschrig, T. K. Kim, and M. D. Watson, FeSe and the missing electron pocket problem, arXiv:2201.11702.

[22] M. D. Watson, A. A. Haghighirad, L. C. Rhodes, M. Hoesch, and T. K. Kim, Electronic anisotropies revealed by detwinned angle-resolved photo-emission spectroscopy measurements of FeSe, New J. Phys. **19**, 103021 (2017).

[23] P. O. Sprau, A. Kostin, A. Kreisel, A. E. Böhmer, V. Taufour, P. C. Canfield, S. Mukherjee, P. J. Hirschfeld, B. M. Andersen, and J. C. S. Davis, Discovery of orbital-selective cooper pairing in FeSe, Science **357**, 75 (2017).

[24] A. Kreisel, B. M. Andersen, P. O. Sprau, A. Kostin, J. C. S. Davis, and P. J. Hirschfeld, Orbital selective pairing and gap structures of iron-based superconductors, Phys. Rev. B **95**, 174504 (2017).

[25] L. C. Rhodes, M. D. Watson, A. A. Haghighirad, D. V. Evtushinsky, M. Eschrig, and T. K. Kim, Scaling of the superconducting gap with orbital character in FeSe, Phys. Rev. B **98**, 180503(R) (2018).

[26] J. Kang, R. M. Fernandes, and A. Chubukov, Superconductivity in FeSe: The Role of Nematic Order, Phys. Rev. Lett. **120**, 267001 (2018).

[27] H. Hu, R. Yu, E. M. Nica, J.-X. Zhu, and Q. Si, Orbital-selective superconductivity in the nematic phase of FeSe, Phys. Rev. B **98**, 220503(R) (2018).

[28] L. C. Rhodes, J. Böker, M. A. Müller, M. Eschrig, and I. M. Eremin, Non-local d_{xy} nematicity and the missing electron pocket in FeSe, npj Quantum Mater. **6**, 45 (2021).

[29] J.-H. Chu, J. G. Analytis, K. D. Greve, P. L. McMahon, Z. Islam, Y. Yamamoto, and I. R. Fisher, In-plane resistivity anisotropy in an underdoped iron arsenide superconductor, Science **329**, 824 (2010).

[30] M. A. Tanatar, E. C. Blomberg, A. Kreyssig, M. G. Kim, N. Ni, A. Thaler, S. L. Bud'ko, P. C. Canfield, A. I. Goldman, I. I. Mazin, and R. Prozorov, Uniaxial-strain mechanical detwinning of $CaFe_2As_2$ and $BaFe_2As_2$ crystals: Optical and transport study, Phys. Rev. B **81**, 184508 (2010).

[31] A. Dusza, A. Lucarelli, F. Pfuner, J.-H. Chu, I. Fisher, and L. Degiorgi, Anisotropic charge dynamics in detwinned $Ba(Fe_{1-x}Co_x)_2As_2$, Europhys. Lett. **93**, 37002 (2011).

[32] I. R. Fisher, L. Degiorgi, and Z. X. Shen, In-plane electronic anisotropy of underdoped "122" Fe-arsenide superconductors revealed by measurements of detwinned single crystals, Rep. Prog. Phys. **74**, 124506 (2011).

[33] A. Dusza, A. Lucarelli, A. Sanna, S. Massidda, J.-H. Chu, I. R. Fisher, and L. Degiorgi, Anisotropic in-plane optical conductivity in detwinned ba(fe1-xcox)2as2, New J. Phys. **14**, 023020 (2012).

[34] C. Mirri, A. Dusza, S. Bastelberger, J.-H. Chu, H.-H. Kuo, I. R. Fisher, and L. Degiorgi, Nematic-driven anisotropic electronic properties of underdoped detwinned $Ba(Fe_{1-x}Co_x)_2As_2$ revealed by optical spectroscopy, Phys. Rev. B **90**, 155125 (2014).

[35] E. C. Blomberg, M. A. Tanatar, R. M. Fernandes, I. I. Mazin, B. Shen, H.-H. Wen, M. D. Johannes, J. Schmalian, and R. Prozorov, Sign-reversal of the in-plane resistivity anisotropy in hole-doped iron pnictides, Nature Commun. **4**, 1914 (2013).

[36] M. A. Tanatar, A. E. Böhmer, E. I. Timmons, M. Schütt, G. Drachuck, V. Taufour, K. Kothapalli, A. Kreyssig, S. L. Bud'ko, P. C. Canfield, R. M. Fernandes, and R. Prozorov, Origin of the Resistivity Anisotropy in the Nematic Phase of FeSe, Phys. Rev. Lett. **117**, 127001 (2016).

[37] R. M. Fernandes, E. Abrahams, and J. Schmalian, Anisotropic In-Plane Resistivity in the Nematic Phase of the Iron Pnictides, Phys. Rev. Lett. **107**, 217002 (2011).

[38] M. Nakajima, S. Ishida, Y. Tomioka, K. Kihou, C. H. Lee, A. Iyo, T. Ito, T. Kakeshita, H. Eisaki, and S. Uchida, Effect of Co Doping on the In-Plane Anisotropy in the Optical Spectrum of Underdoped $Ba(Fe_{1-x}Co_x)_2As_2$, Phys. Rev. Lett. **109**, 217003 (2012).

[39] S. Ishida, M. Nakajima, T. Liang, K. Kihou, C. H. Lee, A. Iyo, H. Eisaki, T. Kakeshita, Y. Tomioka, T. Ito, and S. Uchida, Anisotropy of the In-Plane Resistivity of Underdoped $Ba(Fe_{1-x}Co_x)_2As_2$ Superconductors Induced by Impurity Scattering in the Antiferromagnetic Orthorhombic Phase, Phys. Rev. Lett. **110**, 207001 (2013).

[40] M. P. Allan, T.-M. Chuang, F. Massee, Y. Xie, N. Ni, S. L. Bud'ko, G. S. Boebinger, Q. Wang, D. S. Dessau, P. C. Canfield, M. S. Golden, and J. C. Davis, Anisotropic impurity states, quasiparticle scattering and nematic transport in underdoped ca(fe1-xcox)2as2, Nat. Phys. **9**, 220 (2013).

[41] M. Schütt, J. Schmalian, and R. M. Fernandes, Origin of dc and ac conductivity anisotropy in iron-based superconductors: Scattering rate versus spectral weight effects, Phys. Rev. B **94**, 075111 (2016).

[42] S. Onari and H. Kontani, In-plane anisotropy of transport coefficients in electronic nematic states: Universal origin of nematicity in Fe-based superconductors, Phys. Rev. B **96**, 094527 (2017).

[43] H.-H. Kuo and I. R. Fisher, Effect of Disorder on the Resistivity Anisotropy Near the Electronic Nematic Phase Transition in Pure and Electron-Doped $BaFe_2As_2$, Phys. Rev. Lett. **112**, 227001 (2014).

[44] C. Mirri, A. Dusza, S. Bastelberger, M. Chinotti, L. Degiorgi, J.-H. Chu, H.-H. Kuo, and I. R. Fisher, Origin of the Resistive Anisotropy in the Electronic Nematic Phase of $bafe_2as_2$ Revealed by Optical Spectroscopy, Phys. Rev. Lett. **115**, 107001 (2015).

[45] C. Mirri, A. Dusza, S. Bastelberger, M. Chinotti, J.-H. Chu, H.-H. Kuo, I. R. Fisher, and L. Degiorgi, Electrodynamic response in the electronic nematic phase of $BaFe_2As_2$, Phys. Rev. B **93**, 085114 (2016).

[46] M. Breitkreiz, P. M. R. Brydon, and C. Timm, Transport in multiband systems with hot spots on the Fermi surface: Forward-scattering corrections, Phys. Rev. B **89**, 245106 (2014).

[47] M. Chinotti, A. Pal, L. Degiorgi, A. E. Böhmer, and P. C. Canfield, Optical anisotropy in the electronic nematic phase of FeSe, Phys. Rev. B **96**, 121112(R) (2017).

[48] L. Benfatto and E. Cappelluti, Effects of the fermi-surface shrinking on the optical sum rule in pnictides, Phys. Rev. B **83**, 104516 (2011).

[49] L. Benfatto, E. Cappelluti, L. Ortenzi, and L. Boeri, Extended drude model and role of interband transitions in the midinfrared spectra of pnictides, Phys. Rev. B **83**, 224514 (2011).

[50] R. Fernández-Martín, L. Fanfarillo, L. Benfatto, and B. Valenzuela, Anisotropy of the dc conductivity due to orbital-selective spin fluctuations in the nematic phase of iron superconductors, Phys. Rev. B **99**, 155117 (2019).

[51] M. Marciani and L. Benfatto, Boltzmann electronic dc transport in multiorbital weakly disordered crystals, Phys. Rev. B **104**, 235143 (2021).

[52] G. D. Mahan, *Many Particle Physics*, 3rd ed. (Plenum, New York, 2000).

[53] V. Cvetkovic and O. Vafek, Space group symmetry, spin-orbit coupling, and the low-energy effective hamiltonian for iron-based superconductors, Phys. Rev. B **88**, 134510 (2013).

[54] J. M. Ziman, *Electrons and Phonons: The Theory of Transport Phenomena in Solids*, International series of monographs on physics (Clarendon Press, Oxford, 1960).

[55] E. H. Sondheimer, The boltzmann equation for anisotropic metals, Proc. R. Soc. London A **268**, 100 (1962).

[56] P. L. Taylor, The boltzmann equation for conduction electrons, Proc. R. Soc. London A **275**, 200 (1963).

[57] Y. Wu and N. Goldsman, An efficient solution of the multi-band boltzmann transport equation in silicon, COMPEL **12**, 475 (1993).

[58] T. G. S. M. Rijks, R. Coehoorn, M. J. M. de Jong, and W. J. M. de Jonge, Semiclassical calculations of the anisotropic magnetoresistance of NiFe-based thin films, wires, and multilayers, Phys. Rev. B **51**, 283 (1995).

[59] V. Brosco, L. Benfatto, E. Cappelluti, and C. Grimaldi, Unconventional dc Transport in Rashba Electron Gases, Phys. Rev. Lett. **116**, 166602 (2016).

[60] E. Bringuier, The boltzmann equation and relaxation-time approximation for electron transport in solids, Eur. J. Phys. **40**, 025103 (2019).

[61] M. Nakajima, S. Ishida, T. Tanaka, K. Kihou, Y. Tomioka, T. Saito, C. H. Lee, H. Fukazawa, Y. Kohori, T. Kakeshita, A. Iyo, T. Ito, H. Eisaki, and S. Uchida, Normal-state charge dynamics in doped $BaFe_2As_2$: Roles of doping and necessary ingredients for superconductivity, Sci. Rep. **4**, 5873 (2015).

[62] M. Ghini, M. Bristow, J. C. A. Prentice, S. Sutherland, S. Sanna, A. A. Haghighirad, and A. I. Coldea, Strain tuning of nematicity and superconductivity in single crystals of fese, Phys. Rev. B **103**, 205139 (2021).

[63] M. Bristow, P. Reiss, A. A. Haghighirad, Z. Zajicek, S. J. Singh, T. Wolf, D. Graf, W. Knafo, A. McCollam, and A. I. Coldea, Anomalous high-magnetic field electronic state of the

nematic superconductors fese$_{1-x}$s$_x$, Phys. Rev. Research **2**, 013309 (2020).

[64] L. Fanfarillo, E. Cappelluti, C. Castellani, and L. Benfatto, Unconventional Hall Effect in Pnictides from Interband Interactions, Phys. Rev. Lett. **109**, 096402 (2012).

[65] A. E. Böhmer, F. Hardy, F. Eilers, D. Ernst, P. Adelmann, P. Schweiss, T. Wolf, and C. Meingast, Lack of coupling between superconductivity and orthorhombic distortion in stoichiometric single-crystalline FeSe, Phys. Rev. B **87**, 180505(R) (2013).